Real-time plasmonic monitoring of electrocatalysis on single nanorods

Wang, Jun-gang; Fossey, John S.; Li, Meng; Li, Da-wei; Ma, Wei; Ying, Yi-lun; Qian, Ruo-can; Cao, Chan; Long, Yi-tao

DOI:
10.1016/j.jelechem.2016.10.008

Real-time plasmonic monitoring of electrocatalysis on single nanorods

Jun-Gang Wang, John S. Fossey, Meng Li, Da-Wei Li, Wei Ma, Yi-Lun Ying, Ruo-Can Qian, Chan Cao, Yi-Tao Long

PII: S1572-6657(16)30529-X
DOI: doi:10.1016/j.jelechem.2016.10.008
Reference: JEAC 2875

To appear in: *Journal of Electroanalytical Chemistry*

Received date: 25 May 2016
Revised date: 29 September 2016
Accepted date: 5 October 2016

Please cite this article as: Jun-Gang Wang, John S. Fossey, Meng Li, Da-Wei Li, Wei Ma, Yi-Lun Ying, Ruo-Can Qian, Chan Cao, Yi-Tao Long, Real-time plasmonic monitoring of electrocatalysis on single nanorods, *Journal of Electroanalytical Chemistry* (2016), doi:10.1016/j.jelechem.2016.10.008

Real-Time Plasmonic Monitoring of Electrocatalysis on Single Nanorods

Jun-Gang Wang[†], John S. Fossey[‡], Meng Li[†§], Da-Wei Li[†], Wei Ma[†], Yi-Lun Ying[†], Ruo-Can Qian[†], Chan Cao[†], and Yi-Tao Long[†*]

[†]Key Laboratory for Advanced Materials & Department of Chemistry, East China University of Science and Technology, 130 Meilong Road, Shanghai, 200237, P. R. China.

[‡]School of Chemistry, University of Birmingham, Edgbaston, Birmingham, West Midlands, B15 2TT, U.K.

[§]State Environmental Protection Key Laboratory of Risk Assessment and Control on Chemical Processes, East China University of Science and Technology, Shanghai 200237, P. R. China.

Abstract

Changes in the optical properties of single gold nanorods during electrocatalytic oxidation of glucose in alkaline media are monitored in real-time by single-nanoparticle dark-field spectroelectrochemistry. The spectral scattering characteristics under dynamic potential scan conditions are closely related to the electrochemical processes, and the electrochemical catalytic mechanism of the process is discussed. Moreover, changes in free-electron density are evaluated using a Drude dielectric function with charge density-modification. The proposed sensing technique based on plasmonic analysis shows significant promise for the design and research of electrochemical catalytic systems at the single-nanoparticle level.

Keywords: *local chemical reaction, localized surface plasmon resonance, spectroelectrochemistry, single nanoparticle*

1. Introduction

Localized surface plasmon resonances (LSPR) are collective oscillations of conduction band electrons in a metal nanoparticles.[1] Recently, the study of LSPR properties of noble metal nanostructures has lead to significant advances and new applications in nanophotonic devices and circuits,[2-4] plasmonic waveguides,[5] Fano resonances,[6, 7] surface enhanced spectroscopy,[8-10] plasmonic nanoantennas,[11] solar energy conversion,[12-14] biological sensing and imaging,[15-18] and in life sciences.[18-23] A nanoparticle's size, shape, electron density and dielectric (electronic) properties as well as its dielectric environmental changes can influence its LSPR properties.[24] Charge transfer and storage processes have been a growing focus, and understanding fundamental aspects of the physical and chemical process governing charge transfer at the nanoscale is of paramount importance.[25] Noble metal nanostructures have served as a heterogeneous catalyst in various chemical transformations, from the synthesis of fine chemicals through pollutant removal to electrochemical cells for energy conversion.[26, 27] In order to investigate electrochemical catalytic reactions by plasmonic spectroelectrochemistry techniques, bifunctional noble metal structures that have plasmonic properties and can serve as a catalyst are required.[28] It is critical that nanoparticle size, shape and composition are considered when engineering nanocatalysts. Especially considering that

nanocatalysts are often inhomogeneous and this can lead to heterogeneity in the electrochemical catalytic activity. Therefore, only average efficiency is obtained by ensemble catalytic measurements. To effectively study these catalytic processes and eliminate ensemble averaging, single particle spectroscopy techniques are required.[29] This coupled with the fact that it is extremely challenging to study heterogeneous catalytic redox systems on noble metal nanocrystal surfaces means a single particle approach is especially pertinent.

Numerous factors influence catalytic surface reaction processes including surface area, facets and composition.[27] Model systems with single-crystalline facets have been studied under idealised ultrahigh vacuum conditions.[30, 31] For instance, gold nanorods have served as model catalysts providing information on aspects of reactions catalysed by oxidation of ascorbic acid on a gold nanocrystal surface, including features such as charge transfer steps.[32, 33] In order to further understand and improve these systems, it is important to monitor catalysis in real time.[34] However, conventional surface interrogation techniques usually require high-vacuum conditions or are limited to ensemble average measurement with high cost.[35] It is a major challenge to correlate the results obtained from model systems or artificial reaction regimes to nanostructure catalysis under real reaction conditions.[27]

Herein, a novel plasmonic spectroelectrochemistry technique for the study electrocatalytic reactions *in situ* is revealed. Plasmonic spectral characteristics are used to ascertain information on electrocatalytic reactions occurring at noble metal nanoparticles under dynamic potential control (Figure 1). Electrocatalytic oxidation of glucose in alkaline media was chosen as a suitable and important model reaction, not least due to the potential for exploitation of glucose as a next generation energy source.[36],[34] As such the electrocatalytic oxidation of glucose at single particle level is investigated for the first time. LSPR spectral changes are correlated to catalytic reaction steps, which can be used to postulate the electrochemical redox reaction mechanism at single-nanoparticle level.

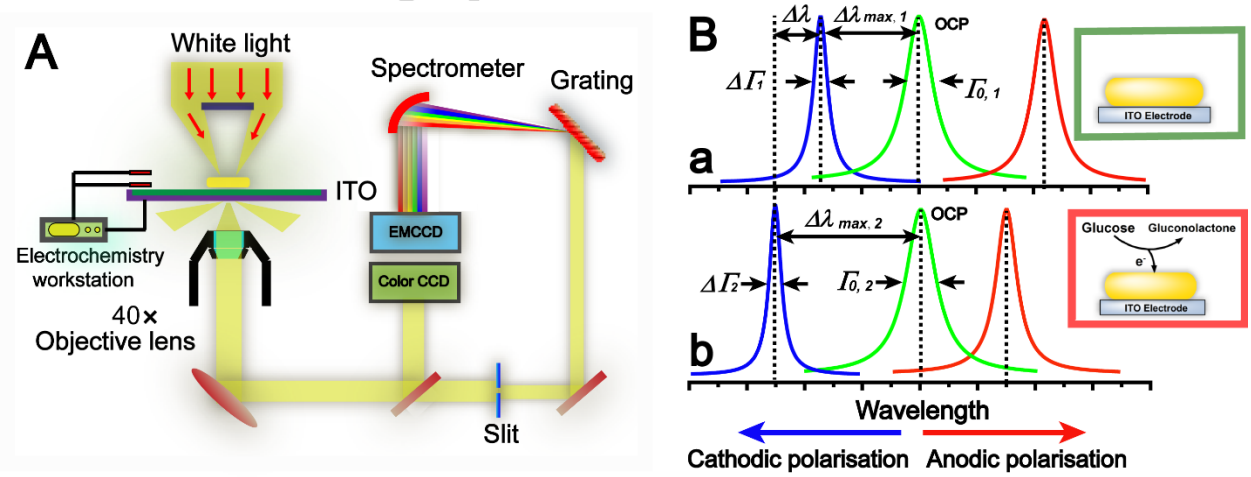

Figure 1. (A) Experimental setup for single nanoparticle plasmon spectroelectrochemistry: dark-field microscopy coupled with an electrochemical workstation. (B) Schematic representation of the direct localized plasmon sensing strategy and real-time monitoring of single-nanoparticle electrochemical catalysis. Scattering spectra *versus* wavelength at different polarisation potentials are shown in the absence (a) and presence (b) of glucose, respectively.

The scattering spectrum (green line) of a single gold nanorod shown in (a) and (b) was obtained at open circuit potential (OCP). Scattering spectra (red and blue lines) were obtained under anodic polarisation and cathodic polarisation, respectively. Spectral shifts, $\Delta\lambda_{max}$, and changes in the peak full-width at half maximum (Δfwhm, $\Delta\Gamma$) induced by catalysis serve as a readout providing information on the electrocatalytic oxidation of glucose on the single gold nanorod. The λ_{max} and Γ obtained at OCP in the absence and presence of glucose serve as reference points to calcualte the $\Delta\lambda_{max}$ and $\Delta\Gamma$.

2. Experimental

2.1 Materials

Indium tin oxide (ITO)-coated glass sheets (sheet resistances 20-30 Ω sq^{-1}; 1 mm thickness) purchased from Shenzhen Laibao hi-tech Co. LTD (Shenzhen China),were cut into small pieces (20 mm × 20 mm) and coated with a polydimethylsiloxane (PDMS) cell to serve as the working electrode. Potassium hydroxide (KOH), acetone (AR), isopropanol (AR), ethanol (AR) and potassium chloride (KCl) were purchased from Sinopharm Chemical Reagent Co., Ltd (Shanghai China). Glucose was purchased from Sigma-Aldrich Co. Gold nanorods (40 nm; 65 nm; 10 O.D.) were purchased from Nanoseedz (Hong Kong, China). The dimensions of the gold nanorod used in this study were 44 ± 3 nm in length and 98 ± 6 nm in diameter (n > 150) as characterised by transmission electron microscopy (TEM, JEOL JEM-2100, Japan). All reagents were of analytical grade and used as received without any further purification. Ultrapure water, filtered by a Milli-Q reagent water system at a resistivity of > 18MΩ cm, was used throughout the experiments. The ITO-coated glass was cleansed first by ethanol, and then washed successively in acetone, isopropanol and pure water with at least 30 min sonication. Lastly they were dipped in a mixture of pure water, hydrogen peroxide and ammonium hydroxide (volume ratio, 5:1:1) and heated to boiling for at least 30 min,[10] and then dried with nitrogen gas. Gold nanorods were immobilised on the ITO electrodes through electrostatic adsorption by placing the

ITO electrode in the diluted gold nanorod solution (300 times) for 5 min. Then, the gold nanorod modified ITO electrodes were rinsed with copious amounts of water prior to dark-field measurements. The gold nanorod modified ITO electrodes were stable to cyclic voltammetric scanning, as shown in the Figure S1.

2.2 Instrumentation

2.2.1 Electrochemistry

All electrochemical experiments were performed on a CHI660E electrochemical workstation (CH Instruments Inc.) in a conventional one-compartment cell in conjunction with a standard three-electrode system. A PDMS microelectrochemical flow cell was used in the electrochemical experiments (Schematic S1). ITO electrodes modified with gold nanorods served as the working electrode. A Pt wire electrode served as the counter electrode and another Pt wire electrode functioned as reference electrode. The potential of the Pt reference electrode was calibrated through a cyclic voltammetry scan of potassiumferricyanide (Figure S2, Supporting Information). The $\Delta E_0^{1/2}$ was 0.4 mV between using Pt quasi-reference electrode and saturated calomel reference electrode (SCE) in 5.00 mM $K_3[Fe(CN)_6]$ solution, respectively. Ensemble gold nanorods modified ITO electrodes were prepared by spin-coating three drops of gold nanorods solution onto an ITO electrode (geometry area *ca*. 0.50 cm^2). Experiments were carried out with KOH as the supporting electrolyte, and the solutions were purged with nitrogen (20 min) before electrochemical experiments. All solutions were stored under an atmosphere of nitrogen and all experiments were performed at room temperature 25 ± 2 °C.

2.2.2 Dark-Field Microspectroscopy

Optical dark-field spectrum measurements were recorded using a Nikon eclipse Ti-U inverted microscope equipped with a dark-field condenser (0.8 < NA < 0.95) and a 40 × objective lens (NA = 0.8). Illumination was provided by a 100 W halogen lamp which was used to excite the gold nanorods generating the local plasmon resonance scattering light. The scattering light was focused onto the entrance port of a monochromator (Isoplane SCT 320) that was equipped with a grating (grating density: 300 lines/ mm; blazed wavelength: 500 nm) to disperse the scattering light. Then, the scattering light was recorded by a 400 × 1600 pixel cooled spectrograph CCD camera (ProEM+: 1600eXcelon3, Princeton Instruments, USA). A true-color digital camera (Nikon, DS-fi, Japan) was used to record the field of the microscope for coregistration with the monochromator. Adjustable entrance slits can be opened to retain only a single gold nanorod in the region of interest. Note that a distribution of spacings between gold nanorods can be produced in the sample preparation. The scattering spectra from single gold nanorods were corrected by subtracting the background spectra taken from the adjacent regions, without the gold nanorods and dividing with the calibrated response curve of the entire optical system. To ensure that only optically isolated gold nanorods were analysed, only scattering with smooth baseline, a single Lorentzian peak and a non-distorted line shape were accepted.[37] The integration time used in all experiments spectral acquisitions was 5 seconds.

3. Results and Discussion

3.1 Scattering Spectra of Single Gold Nanorods

Typical TEM images of gold nanorods and the associated size distribution histograms (length and width) for the gold nanorods are presented in Figure S3 (Supporting Information). A

typical spectrum of single gold nanorod at an open circuit potential corresponding to red colour and the local electric field distribution of the single nanorod (98 nm × 44 nm) using the discrete dipole approximation (DDA) method are shown in Figure S4.[38] The line width (Γ) of the resonance of a single plasmonic nanoparticle was sensitive to changes in environment (eq. S1-6). The change of line width could also reflect the physical and chemical process occurring in the proximity of plasmonic nanostructures due to changes of their plasmon properties, because the refractive index around the nanostructure and free electron density was greatly dependent on these processes.[39] A quantitative description of the cross sections of nanoparticles excited by polarised light parallel to the principle axes are given in eq. S7-9.

3.2 Electrocatalytic Process of Glucose Oxidation on Single Gold Nanorods in Alkaline Media

The electrochemical behavior of a gold nanorod-modified ITO electrode was initially probed using cyclic voltammetry (Figure S5-7). In alkaline solution, excellent electrocatalytic oxidation activity towards glucose was observed. Next, real-time monitoring of dark-field spectroelectrochemistry (SN-DFS) changes in a single gold nanorod's optical properties was investigated. Scattering spectra for a single nanorod (*ca.* 98 nm × 44 nm) showed a slight spectral shift associated with a spectral line width change due to oxidation of glucose (Figure 2, A and B). This spectral peak shift demonstrates that physicochemical properties of the nanorod surface state is interrogated by this technique.[23] In addition, plasmon resonance energy was modulated by applied potential. The dark-field scattering spectrum was measured at open circuit potential (- 0.14 V) prior to the application of a potential step sequence to the electrode. No

obvious spectral changes ($\Delta\lambda_{max}$ and $\Delta\Gamma$) were observed at open circuit potential in the absence and presence of glucose, respectively (Figure S8). This demonstrates that there was no auto-oxidation of glucose in the gold nanorod ITO system in alkaline media.

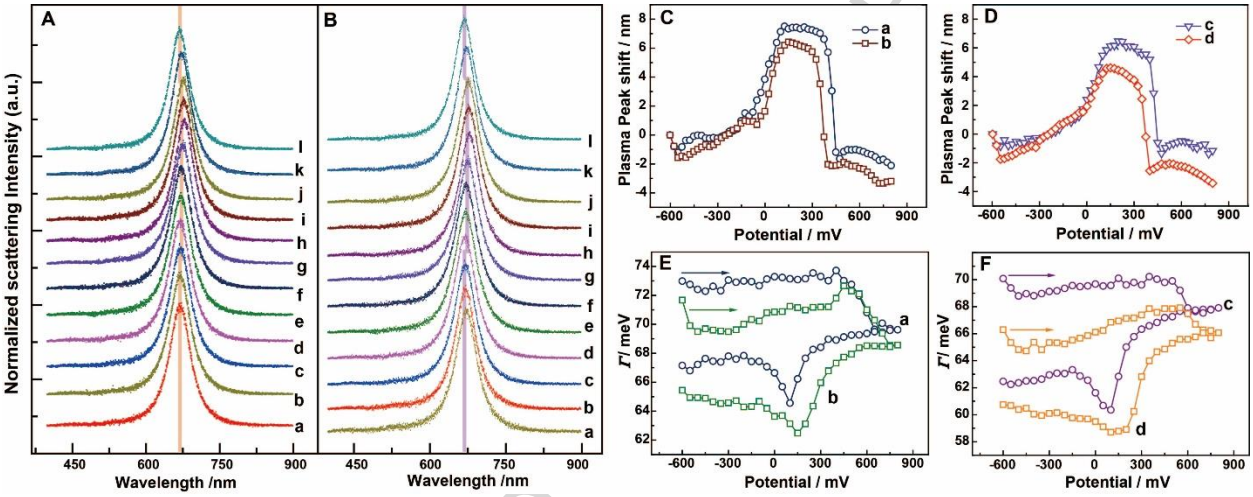

Figure 2. (A) and (B) Normalized scattering spectra for a single gold nanorod on a modified ITO electrode under dynamic potential control in the absence and presence of glucose, respectively. (Note: spectra are stacked for clarity.) The solid lines show the fits to the scattering spectra using a Lorentzian function. The potentials were at open circuit potential, -500 mV, -350, 150, 450, 550, 700 mV (a, b, c, d, e, f and g, respectively) then back to 650, 400, 200, 100, -200 mV (h, i, j, k and l, respectively). The shading represents the trend of the plasma spectral shifts during the dynamic potential scan. (C, D) Plasma peak shifts ($\Delta\lambda_{max}$) and (E, F) changes in the peak full-width at half maximum (fhwm, Γ) are shown for two kinds of single gold nanorods with distinctive scattering resonant wavelengths, 670 nm (a, b) and 650 nm (c, d), *versus* applied potential. Curve a and c were obtained in 0.5 M KOH solution and b and d were in the 0.5 M KOH + 10 mM glucose.

To investigate the catalytic mechanism on a single gold nanorod, potential dependent dark-field scattering spectra peak shift, $\Delta\lambda_{\max}$ of two types of single gold nanorods, were measured during dynamic potential scanning (Figure 2C, D). From -0.6 V to -0.5 V the LSPR peak position underwent a blue shift of 2 nm in 10 s (Figure 2C, a). The blue shift was attributed to a double-layer charging process or an electronic charging effect.[40] Electrons are transferred from the conductive ITO electrode to the gold nanorods, which induces a net negative charge,

corresponding to a higher free electron density than in the natural state.[25] The surface of the gold nanorod is covered by hydrated cations forming a positively charged Stern layer.[41] When the potential reached to the potential of zero charge (E_{PZC}) ca. 0.1 V, there is no net negative or positive charge on the single nanorod because no scattering spectral shift was observed during potential scan.[42] Then, electrons are extracted from the single nanorod under investigation due to double layer charging. This leads to a lowering of the free electron density from 0.10 V to 0.3 V. A negatively charged Stern layer (pre-oxidation) is composed of hydrated hydroxide ions to screen the positively charged gold surface. This pre-oxidation layer led to increasing the double layer capacitance, according to the Grahame model.[25, 43, 44] Thereafter, a quasi-linear dependence of the peak shift on the applied potential was found in the potential range from 0.4 V to 0.8 V. The gold began to oxidise forming a hydrated gold hydroxide layer and a further spectral red shift was observed with a sensitivity of 15.9 nm V^{-1}. The thickness of hydrated gold hydroxide ($Au(OH)_{ads}^{(1-\lambda)-}$) layer has a linear growth property with applied anodic polarisation from 0.4 V to 0.8 V. At 0.8 V, a 7.1 nm red shift was observed (Figure 2C, a), however, only a 5.8 nm red shift was found at 0.8 V (Figure 2D, c) for single nanorod with scattering peak wavelength 650 nm. These results may be interpreted by assuming that gold nanorods with a larger aspect ratio are more sensitive to changes of the surface medium.[45] During cathodic scan from 0.8 V to 0.3 V, the spectra had a balanced domain with a slight blue shift (ca. 0.5 nm). It was due to the steady property of the $Au(OH)_{ads}^{(1-\lambda)-}$ in weak cathodic polarization from 0.8 to 0.3 V and we can find there is no obvious reduction current for Au nanorods (Figure 3C). When the potential was decreased to 0.3 V, there was a blue shift of the LSPR induced by reduction of the $Au(OH)_{ads}^{(1-\lambda)-}$ to form $[Au^{+}(H_2O)_n]_{ads}$ on the gold surface, which then possessed catalytic

activity to glucose oxidation with associated electron injection into the gold nanorod.[46] The scattering spectral shift showed a weak spectral shift sensitivity of -1.53 nm V^{-1} in cathodic polarisation scope from 0.05 V to -0.6 V, because the free electron density in the gold nanorod has reached saturation which is not significantly affected by the injection of electrons in persistent cathodic polarisation.[47, 48]

The scattering spectral shift in presence of glucose (Figure 2C, b) indicated a slight blue shift of LSPR compared to that in the absence of glucose (Figure 2C, a). Due to the double layer charging effect, a *ca*. 2 nm blue shift was observed in the potential range from -0.6 to -0.5 V (Figure 2C, b). Anodic polarisation with a more intense blue shift was found over -0.5 to 0.1 V. Double layer charging and Faradaic processes were involved the glucose catalytic oxidation which led to a change of free electron density in the gold nanorods. This intense spectral blue shift was composed of both double layer charging and Faradaic processes. During anodic discharge processes from 0.1 to 0.3 V, the scattering spectral peak shifts has a linear increase relationship with the applied potential. With anodic polarisation, a sharp rise of the $\Delta\lambda_{max}$ from 0.3 to 0.8 V with a sensitivity of 18.3 nm V^{-1} was found, which was more pronounced than that in the absence of glucose due to the oxidation of glucose leading the free electron density increase. The scattering spectra of single gold nanorods with short aspect ratios, in absence and presence of glucose (Figure 2D, curve c and d), showed weaker scattering spectral shift than gold nanorods with long aspect ratios (Figure 2C, curve a and b). This demonstrated that larger aspect ratio gold nanorods are more sensitive to the medium and free electron density changes. In addition, the gold nanorods with different scattering spectral peak wavelength indicated various peak red shifts (Figure S9). These results demonstrated that the heterogeneity in size and shape

of individual gold nanorods caused their differing ability to electrochemically catalyze the oxidation of glucose. Gold nanorods with similar scattering spectra peak wavelength may have very different results during catalytic reaction as shown in Figure S9 (B: λ_p= 689 nm; D: λ_p = 690 nm and G: λ_p = 690). The single-nanoparticle dark-field spectroelectrochemistry technique provides an effective protocol in high-throughput screening of catalysts.[44] A dynamic simulation of the gold electrochemical oxidation process is shown in Figure S10. In alkaline media, anodic polarisation of the gold nanorods takes place, leading to the formation of $Au(OH)_{ads}^{(1-\lambda)-}$ on the gold surface. The spectral shift ($\Delta\lambda_{max}$) is caused by the formation of $Au(OH)_{ads}^{(1-\lambda)-}$ on the surface of the gold nanorod and the magnitude of the peak shift comes from the amount of the $Au(OH)_{ads}^{(1-\lambda)-}$. The scattering spectral shift ($\Delta\lambda_{max}$) in the gold nanorod oxidation process are proportional to $t^{3/2}$ during dynamic potential scan. Nevertheless, in cathodic polarisation $\Delta\lambda_{max}$ changed with time following the trend t^2- $(t\text{-}t_c)^3$ (Supporting Information, section S3). The relationship between scattering spectral shift and time demonstrated that the spectral shift was influenced by the chemical composition of the surface of the gold nanrods as well as the range of the potential scan.[49]

When the sample material is subject to some alteration due to some inherent change of the noble metal itself, the dielectric properties or free electron density change could cause measurable shifts of the spectral peak position ($\Delta\lambda_{max}$) or of the peak line width ($\Delta\Gamma$) of the gold reporter's LSPR peak.[50] The homogeneous line width of the single gold nanorod's scattering spectra was monitored by the SN-DFS technique, avoiding inhomogeneous broadening effects witnessed during ensemble measurements. The line width of the plasmon resonance (Γ) was influenced by the electron oscillation dephasing processes and the dielectric function of the

particles.[50] Hence, variation in line width of the LSPR during dynamic potential modulation is a valuable parameter for providing information about plasmonic properties.[37, 51, 52] Four different regions were identified in the line width change of a gold nanorod during the potential sweep (Figure 2E, a). In the first region ranging from -0.6 V to 0.4 V, the damping remained essentially constant, consistent with a previous report.[42] In the second region ranging from 0.4 V to 0.65 V, the linearity in the spectral peak red shift coincided with a dramatic decrease of the damping constant, a subsequent cathodic sweep did not lead to a hysteresis loop.[41, 42] In the third region ranging from 0.65 to 0.1 V, there was a nonlinear dependence of the Γ on the applied potential with a gradual depression. With reduction of the $Au(OH)_{ads}^{(1-\lambda)-}$ formed on the surface of gold, the number of the sp-band electrons increased for free movement in oscillation. The relative change in the free electron density ($\Delta N/N$) was - 2.25 % (at 0.8 V) which increased to -2.10 % (at 0.4 V) (Figure S12). The result was comparable to that previously reported, indicating that sp-band electrons are released during cathodic polarization.[26] During the reverse scan in the pre-oxidation region from 0.4 to 0.1 V, there was a sharp increase in $\Delta N/N$, and it transformed from – 2.10 to + 0.50 %. Double layer charging produced *ca*. 0.5 % change in free electron density. The intense decrease of the damping with the cathodic polarisation suggested a decrease of hydration of the gold surface, which decreased the adsorbate damping effect. In addition, sp-band electrons could not be readily excited to the higher energy level of the hybridisation state.[24, 53] When the potential reached to E_{PZC}, ion adsorption on the interface of gold nanorods was restrained in the maximal degree and chemical interface damping was suppressed due to the weak ion adsorption at the potential of zero charge. Therefore, the interface damping (Γ_c, eq. S1-6) was weakened which was due to the low degree of ion

adsorption at gold surface at E_{PZC} point.[54] Finally, below E_{PZC}, an apparent increase of the damping constant was found from 0.1 V to - 0.6 V. Meanwhile, adsorption of hydroxide ions and hydration was decreased and the re-attachment of cations took place. According to the Jellium model, sp-band electrons restrict the water molecules from forming hydrogen bonds with hydroxide ions physisorbed on the gold nanorod.[55] Hence, the hydration of the gold surface was decreased during scanning the potential in the range below E_{PZC}.[56] In the cathodic polarisation experiment below E_{PZC}, the increase in Γ was attributed to re-adsorption of the cations that resulted in plasmon oscillation damping. This was accompanied by inward diffusion of ions and efficient charging of the inner Helmholtz layer around the gold nanorod.[57] The scattering spectral line width of a gold nanorod in the presence of glucose (Figure 2E, b) demonstrated a decrease of the damping constant compared to that in presence of glucose (Figure 2E, a). There was a minimum value point at 0.15 V, which is more positive than that in the absence of glucose. The catalytic oxidation of glucose contributed to this transition, because the injection of electrons during the electrochemical catalytic oxidation of glucose increased the density of free electron in gold nanorod that decreased the damping constant.[50] As shown in Figure 2F, the gold nanorods with initial scattering peak wavelength 650 nm showed various peak linewidth changes after their oxidation and catalysis process compared to gold nanorod (670 nm). These results confirmed that the heterogeneity in size and shape of individual gold nanorods caused their differing ability to electrochemically catalyze the oxidation of glucose.

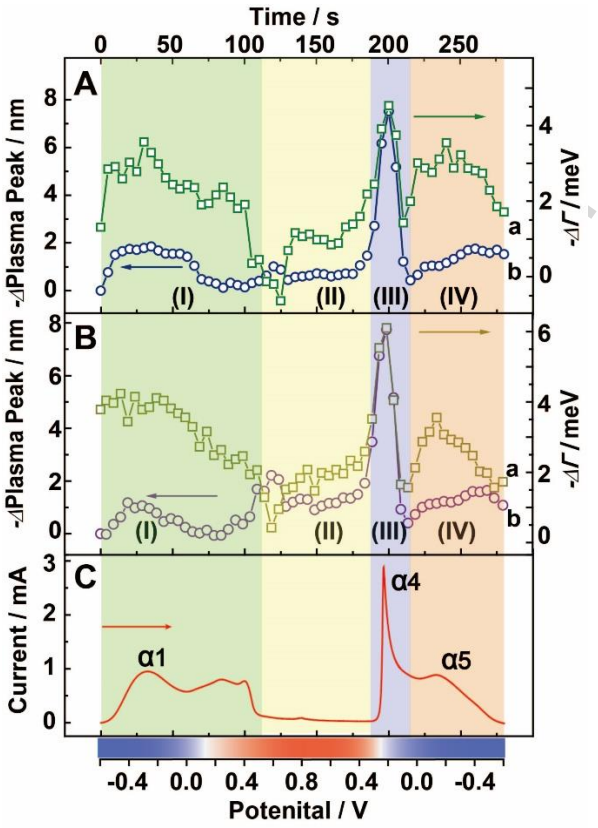

Figure 3. Changes of damping *Γ (ΔΓ)* (a) and change in plasmon resonance peak shift (*Δ*plasma peak) (b) for two kinds of single gold nanorods with distinctive scattering resonant wavelengths, 670 nm (A) and 650 nm (B) between in the absence and presence 10 mM glucose in 0.5 M KOH *versus* applied potential with applied electrochemical scan. (C) CV curve obtained for the Au NR/ITO electrode (ensemble state) in 0.5 M KOH + 10 mM glucose. The spectral blue and red shifts in anodic and cathodic polarisation is represented by blue and red coloured regions for clarity.

To evaluate the effect of the glucose oxidation (Faradaic reaction) on the plasmon properties of single gold nanorods, $\Delta\lambda_{max}$ and $\Delta\Gamma$ were observed in the absence of glucose on single gold nanorod, which was used as the background and subtracted from the data obtained in the presence of glucose. This calibration treatment provided a unique local optical measurement of the charge transfer and the surface state transition, which is extremely difficult to obtain by other approaches.[52] Gold nanorods served not only as the catalysts but also as the plasmonic

reporters in this catalysed reaction. This is different from the plasmonic antenna strategy by Alivisatos and co-workers, who reported that a triangular gold nanoprism acted as a plasmonic sensor while a palladium nanoparticle, in the vicinity, underwent hydrogen gas uptake.[58] Four different regions were identified in the spectral shift and line width change of a gold nanorod in absence and presence of glucose (Figure 3A, B). As shown in Figure 3A, in the first region, the scattering spectral shift with a relatively weak blue shift *ca*. 1.8 nm during the anodic polarisation scan and a peak located at - 0.2 V was found, that fell in line with the peak α1 (Figure 3C). This scattering spectral shift was attributed to the electrosorption of glucose to form adsorbed gluconolactone, releasing one proton per glucose molecule. In the anodic polarisation scan, there were fewer hydroxide ions absorbed on the gold surface.[36] The gold hydroxide served as the catalytic element for glucose oxidation and therefore fewer active sites ($AuOH_{ads}$) are present and a weaker charge transfer takes place between the glucose and the Au surface (Schematic 1, I). Following this adsorption of gluconolactone, the number of the $AuOH_{ads}$ sites are limited which perturbs the oxidation of glucose on the gold surface. Which resulted a slight spectral blue shift at 0.1 V due to the charge transfer suppression between gold nanorod and glucose molecules. In the potential range 0.1 V to 0.4 V, the $\Delta\Gamma$ decreased (*ca*. 2 meV). It is suggested here that in this pre-oxidation potential range, the adsorption of intermediate suppresses the adsorption of hydroxide ions. In addition, the pre-oxidation of Au might possess a larger surface damping constant (Γ_c) than that of the adsorbed intermediate. Above approximately 0.4 V, there was no Faradaic current because of the formation of hydrous Au hydroxide (Schematic 1, II).[36] In the cathodic polarisation, there was a peak of $\Delta\lambda_{max}$ (*ca.* 7.5 nm) at 0.2 V (range, III), this could be due to the regenerated $[Au^{+}(H_2O)_n]_{ads}$ after the reduction

of $[Au_2(H_2O)_9^{3-}]_{ads}$ by glucose.[46] The electrostatic interaction between the cationic mediator $[Au^{+}(H_2O)_n]_{ads}$ and the anionic form of glucose is evidently a major factor in promoting oxidation of glucose at the low potentials in the reverse sweep (Schematic 1, III).[59] This was associated with a peak of reversal damping peak (*ca*. 4.5 meV) located at the same potential (Figure 3A). For the Faradaic processes occurring on the Au surface, electron injection increased free electron density and decreased the damping constant.[60-62] The peak of scattering spectral shift located at 0.2 V was consistent with the incisive current peak α4 at same potential. The transferred electrons injection into a single gold nanorod during glucose electrochemical oxidation reactions alter the plasmon peak wavelength, leading to a blue shift in scattering spectra of the gold nanorod. In range IV from 0.1 to - 0.6 V, the change of the scattering property of the gold nanorod companied by scattering spectral blue shift and an attenuation in line width was attributed to the same mechanism with the peak α1 shown in Schematic 1, I. The current peak α5 corresponding to glucose oxidation was found in the same potential range from 0.1 V to - 0.6 V. The scattering spectra of single gold nanorods with short aspect ratios, in absence and presence of glucose (Figure 3B), showed stronger peak linewidth changes and similar peak shifts compared with gold nanorods with long aspect ratios (Figure 3A). It is noteworthy that it is impossible to study discrepancy of catalytic activity among individual gold nanorods by traditional ensemble electrochemical measurements. The scattering spectral peak shifts and linewidth changes of various gold nanorods with different initial scattering peak wavelength revealed a diversification in catalytic ability during the glucose catalytic oxidation (Figure S9). For the heterogeneity in ratio of different facet, size and shape of various gold nanorods, it brought about inhomogeneous catalytic capacity in the glucose electrocatalytic oxidation. A

change in optical characteristic parameters correlated directly to the ensemble electrochemical current and was critical for probing the local chemical reaction environment. From a more fundamental perspective, electrocatalytic processes could be inferred by the scattering spectral parameters at a single-nanoparticle level thus averting the average effect of traditional measurements.

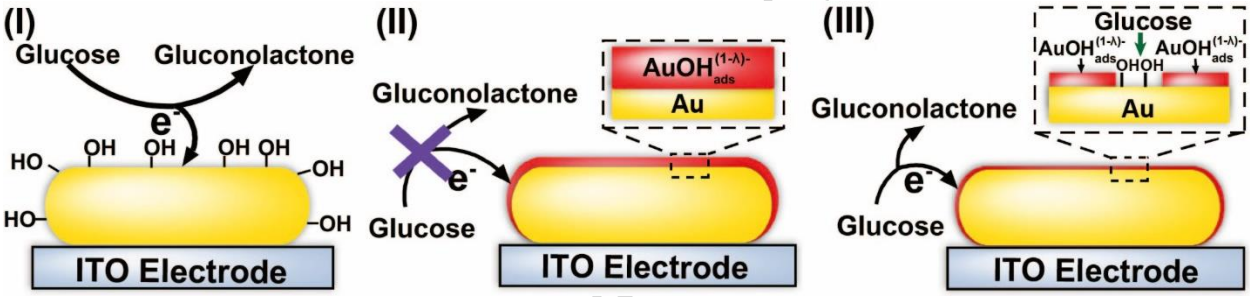

Schematic 1. Schematic representation of the glucose oxidation mechanism and the gold oxidation process occurring at the surface of gold nanorods.

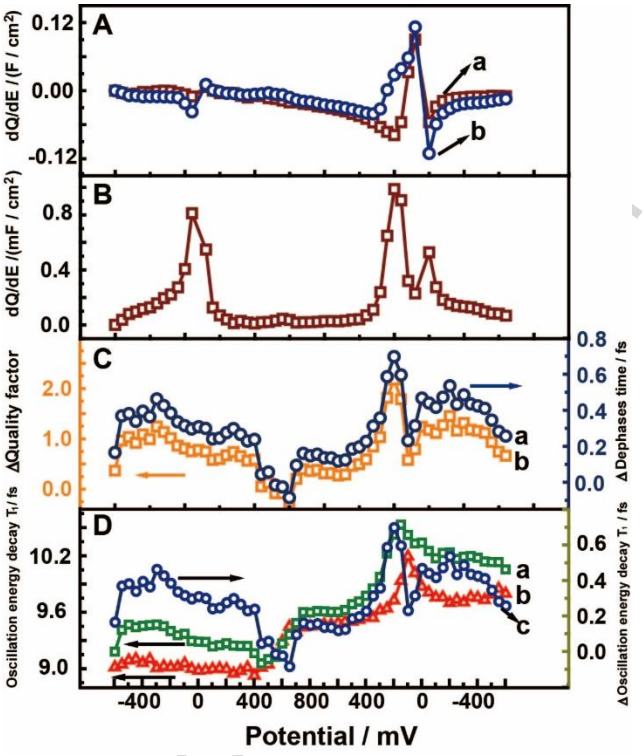

Figure 4. (A) The change of electron density *versus* potential (dQ/dE) noramlised to the single gold nanorod (670 nm) surface area in the absence and presence 10 mM glucose in 0.5 M KOH *versus* applied potential. (B) The differental capacitance (Δ(dQ/dE)) calculated by subtracting the dQ/dE in the absence of glucose from that in the presence glucose obtained from data in (A). (C) Changes of dephasing time T_2 (ΔT_2) (a) and changes of quality factor Q (ΔQ) in the absence and presence 10 mM glucose in 0.5 M KOH. (D) Oscillation energy decay time T_1 (a) and (b) obtained in the absence and presence 10 mM glucose in 0.5 M KOH *versus* applied potential, and changes of ΔT_1 obtained from the single gold nanorod.

To estimate the Faradaic process, the change of electric charge *versus* applied potential (*dQ/dE*) was measured in the absence of glucose as the background and then subtracted from that obtained in the presence of glucose (Figure 4A, B). The change of electron density produced three peaks located at -0.1 V in anodic polarisation, 0.2 and -0.15 V in the cathodic sweep, respectively. This finding is consistent with the potential location of glucose oxidation current peaks (Figure 3C). Plasmon dephasing is characterised by the time constant T_2 and it is associated with the inelastic population time constant T_1, according to the equation $T_2^{-1} = T_1^{-1}/2+$

T^{*-1}, herein, T^{*}described the elastic dephasing process.[63, 64] The quality factor (Q) of the plasmonic nanostructure is one virtue for surface-enhanced Raman scattering spectroscopy (SERS) and it is considered to be related with the electromagnetic enhancement mechanism (EM). The simple equation $T_1 = T_2/2$ for gold nanorods was obtained by neglecting the pure dephasing process that did not contribution to the overall line width.[64] As shown in Figure S13, T_2 ranged from 18.0 to 20.3 fs and the quality factor ranged from 25.4 to 28.7. It was in similar dimensions as reported for gold nanorod at *ca*. 18 fs.[64] Furthermore, El-Sayed and co-workers reported another nonlinear study which demonstrated that the dephasing time of the coherent plasmon oscillation was *ca*. 20 fs.[65] In the negative polarisation scan, T_2 increased monotonically with the peak located at 0.1 V corresponding to the reduction current peak of gold oxide shown in Figure S5A, b. The reduction of the gold oxide decreased the interface damping constant, because the sp-band electrons were released from gold oxide and its' number increased for free movement in oscillation. Nevertheless, reduction in inter-band damping could not be precluded due to the plasmon oscillation energy (1.85 eV) being higher than 1.8 eV.[64] Meanwhile, due to the suppressed interface damping constant, the quality factor had one maximal peak value (28.8) located at 0.1 V the same as T_2. Adjustment of the quality factor was used to improve the electromagnetic enhancement performance of substrate in SERS.[66] In the presence of glucose, electrochemical oxidation of glucose occurred at 0.15 V, leading the increasing of the free electron density in gold nanorod which contributed to the appearance of peak of T_2 and Q at same potential. In the cathodic polarisation, reduction of surface gold oxides occurred at a potential more negative than 0.3 V, where enough surface active sites are available for the direct oxidation of glucose, resulting in a sharp increase in anodic current (0.2 V).[36]

The increase of free electron density during oxidation of glucose contributed to the peaks of ΔT_2 (1.4 fs) and ΔQ (2.2) located at 0.2 V. Therefore, Faradaic currents from glucose oxidation increased the free electron density, and this was attributed to a decrease of damping and the increase of quality factor. Moreover, the respective population decay T_1 in the presence of glucose was longer than that in absence of glucose due to electron injection into the gold nanorods (Figure 4D). In the absence of glucose, the highest population decay time (10.1 fs) was obtained at 0.1 V corresponding to gold oxide reduction. While, the peak point of T_1 (10.5 fs) appeared at 0.15 V associated with the glucose oxidation. The change of oscillation energy decay time T_1 between in absence and presence of glucose (ΔT_1) was proposed to demonstrate the net effect of glucose oxidation on population decay time.[64] The peak (0.70 fs) that was found at 0.2 V was coincident with the peak α4 (Figure 3C). Because the oxidation of glucose increases the free electron density in the gold nanorods which contributed to a decrease of the oscillation energy decay time of gold nanorod. A higher ΔT_1 was a consequence of suppressed interface damping due to electron transfer from glucose to the gold surface during the electrocatalytic reaction.

4. Conclusions

In conclusion, we have demonstrated that the electrocatalytic glucose oxidation on a single gold nanorod is monitored *in situ*, for the first time, by the SN-DFS technique. Potential-dependent LSPR tuning could be used to precisely control the plasmonic properties of gold nanorods. Plasmon peak shift and line width change for the single gold nanorod reporter during glucose oxidation showed significant correlation to ensemble electrochemical

measurements. These plasmonic parameters can be used to reveal the mechanism of heterogeneous catalytic reaction on the noble metal surface. Surface damping and the free electron density significantly depend on the catalytic reaction. This versatile new measurement strategy has promising application in the future to probe different catalytic particles with plasmonic properties. We believe that the results presented here serve as a significant first proof-of-concept for direct nano-sensing of local catalytic processes at the single-nanoparticle level based on plasmonics, and this coupled with electrochemistry offer new insight into many important chemical processes.

Author Information

Corresponding Author

*E-mail: ytlong@ecust.edu.cn. Tel/Fax: 86-21-64252339.

Notes

The authors declare no competing financial interest.

Acknowledgements

Financial support from 973 Program (2013CB733700), the Science Fund for Creative Research Groups (21421004) and Chinese National Foundation of Natural Science Research (21327807) is gratefully acknowledged. The CASE network is thanked for networking opportunities.[67] John S. Fossey thanks ECUST for a Guest Professorship and the University of Birmingham for support.

References

[1] U. Kreibig, M. Vollmer, Optical Properties of Metal Clusters, Vol. 25. Springer Berlin Heidelberg: Brandenburg, 1995.

[2] P. Zijlstra, J.W.M. Chon, M. Gu, Five-dimensional Optical Recording Mediated by Surface Plasmons in Gold Nanorods, Nature 459 (2009) 410-413.

[3] H.A. Atwater, A. Polman, Plasmonics for Improved Photovoltaic Devices, Nat. Mater. 9 (2010) 205-213.

[4] M. Schwind, B. Kasemo, I. Zorić, Localized and Propagating Plasmons in Metal Films with Nanoholes, Nano Lett. 13 (2013) 1743-1750.

[5] J.B. Lassiter, F. McGuire, J.J. Mock, C. Ciracì, R.T. Hill, B.J. Wiley, A. Chilkoti, D.R. Smith, Plasmonic Waveguide Modes of Film-Coupled Metallic Nanocubes, Nano Lett. 13 (2013) 5866-5872.

[6] N.K. Emani, T.-F. Chung, A.V. Kildishev, V.M. Shalaev, Y.P. Chen, A. Boltasseva, Electrical Modulation of Fano Resonance in Plasmonic Nanostructures Using Graphene, Nano Lett. 14 (2013) 78-82.

[7] F. Hao, Y. Sonnefraud, P.V. Dorpe, S.A. Maier, N.J. Halas, P. Nordlander, Symmetry Breaking in Plasmonic Nanocavities: Subradiant LSPR Sensing and a Tunable Fano Resonance, Nano Lett. 8 (2008) 3983-3988.

[8] M. Moskovits, Surface-enhanced Spectroscopy, Rev. Mod. Phys. 57 (1985) 783.

[9] K.A. Willets, Super-resolution imaging of SERS hot spots, Chem. Soc. Rev. 43 (2014) 3854-3864.

[10] J. Wang, X. Cao, L. Li, T. Li, R. Wang, Electrochemical Seed-Mediated Growth of Surface-Enhanced Raman Scattering Active Au (111)-Like Nanoparticles on Indium Tin Oxide Electrodes, J. Phys. Chem. C 117 (2013) 15817-15828.

[11] M.W. Knight, H. Sobhani, P. Nordlander, N.J. Halas, Photodetection with Active Optical Antennas, Science 332 (2011) 702-704.

[12] H. Choi, W.T. Chen, P.V. Kamat, Know Thy Nano Neighbor. Plasmonic versus Electron Charging Effects of Metal Nanoparticles in Dye-Sensitized Solar Cells, ACS Nano 6 (2012) 4418-4427.

[13] P.V. Kamat, Quantum dot solar cells. The Next Big Thing in Photovoltaics, J. Phys. Chem. Lett. 4 (2013) 908-918.

[14] S. Linic, P. Christopher, D.B. Ingram, Plasmonic-metal nanostructures for efficient conversion of solar to chemical energy, Nat. Mater. 10 (2011) 911-921.
[15] B. Xiong, R. Zhou, J. Hao, Y. Jia, Y. He, E.S. Yeung, Highly Sensitive Sulphide Mapping in live cells by kinetic spectral analysis of single Au-Ag core-shell nanoparticles, Nat. Commun. 4 (2013) 1708.
[16] A.S. Stender, K. Marchuk, C. Liu, S. Sander, M.W. Meyer, E.A. Smith, B. Neupane, G. Wang, J. Li, J.-X. Cheng, Single Cell Optical Imaging and Spectroscopy, Chem. Rev. 113 (2013) 2469-2527.
[17] H. Liu, C. Dong, J. Ren, Tempo-Spatially Resolved Scattering Correlation Spectroscopy under Dark-Field Illumination and Its Application to Investigate Dynamic Behaviors of Gold Nanoparticles in Live Cells, J. Am. Chem. Soc. 136 (2014) 2775-2785.
[18] L. Xiao, E.S. Yeung, Optical Imaging of Individual Plasmonic Nanoparticles in Biological Samples, Annu. Rev. Anal. Chem. 7 (2014) 89-111.
[19] P. D. Howes, S. Rana, M. M. Stevens, Plasmonic nanomaterials for biodiagnostics, Chem. Soc. Rev. 43 (2014) 3835-3853.
[20] O. Tokel, F. Inci, U. Demirci, Advances in Plasmonic Technologies for Point of Care Applications, Chem. Rev. 114 (2014) 5728-5752.
[21] S. Carenco, D. Portehault, C. Boissière, N. Mézailles, C. Sanchez, Nanoscaled Metal Borides and Phosphides: Recent Developments and Perspectives, Chem. Rev. 113 (2013) 7981-8065.
[22] K.E. Sapsford, W.R. Algar, L. Berti, K.B. Gemmill, B.J. Casey, E. Oh, M.H. Stewart, I.L. Medintz, Functionalizing Nanoparticles with Biological Molecules: Developing Chemistries that Facilitate Nanotechnology, Chem. Rev. 113 (2013) 1904-2074.
[23] G. Baffou, R. Quidant, Nanoplasmonics for Chemistry, Chem. Soc. Rev. 43 (2014) 3898-907.
[24] B.K. Juluri, M. Lu, Y.B. Zheng, T.J. Huang, L. Jensen, Coupling between Molecular and Plasmonic Resonances: Effect of Molecular Absorbance, J. Phys. Chem. C 113 (2009) 18499-18503.
[25] C.P. Byers, B.S. Hoener, W.-S. Chang, M. Yorulmaz, S. Link, C.F. Landes, Single-Particle Spectroscopy Reveals Heterogeneity in Electrochemical Tuning of the Localized Surface Plasmon, J. Phys. Chem. B 118 (2014) 14047-14055.

[26] M.L. Tang, N. Liu, J.A. Dionne, A.P. Alivisatos, Observations of Shape-Dependent Hydrogen Uptake Trajectories from Single Nanocrystals, J. Am. Chem. Soc. 133 (2011) 13220-13223.
[27] D. Seo, G. Park, H. Song, Plasmonic Monitoring of Catalytic Hydrogen Generation by a Single Nanoparticle Probe, J. Am. Chem. Soc. 134 (2011) 1221-1227.
[28] V. Joseph, C. Engelbrekt, J. Zhang, U. Gernert, J. Ulstrup, J. Kneipp, Characterizing the Kinetics of Nanoparticle-Catalyzed Reactions by Surface-Enhanced Raman Scattering, Angew. Chem. Int. Ed. 51 (2012) 7592-7596.
[29] A. Tcherniak, J.W. Ha, S. Dominguez-Medina, L.S. Slaughter, S. Link, Probing a Century Old Prediction One Plasmonic Particle at a Time, Nano Lett. 10 (2010) 1398-1404.
[30] Y. Bi, S. Ouyang, N. Umezawa, J. Cao, J. Ye, Facet effect of single-crystalline Ag3PO4 sub-microcrystals on photocatalytic properties, J. Am. Chem. Soc. 133 (2011) 6490-6492.
[31] F.F. Tao, S. Zhang, L. Nguyen, X. Zhang, Action of Bimetallic Nanocatalysts under Reaction Conditions and During Catalysis: Evolution of Chemistry from High Vacuum Conditions to Reaction Conditions, Chem. Soc. Rev. 41 (2012) 7980-7993.
[32] C. Novo, A.M. Funston, A.K. Gooding, P. Mulvaney, Electrochemical Charging of Single Gold Nanorods, J. Am. Chem. Soc. 131 (2009) 14664-14666.
[33] C. Novo, A.M. Funston, P. Mulvaney, Direct Observation of Chemical Reactions on Single Gold Nanocrystals Using Surface Plasmon Spectroscopy, Nat. Nanotech. 3 (2008) 598-602.
[34] E.M. Larsson, C. Langhammer, I. Zorić, B. Kasemo, Nanoplasmonic Probes of Catalytic Reactions, Science 326 (2009) 1091-1094.
[35] A. Tittl, X. Yin, H. Giessen, X.-D. Tian, Z.-Q. Tian, C. Kremers, D.N. Chigrin, N. Liu, Plasmonic Smart Dust for Probing Local Chemical Reactions, Nano Lett. 13 (2013) 1816-1821.
[36] J. Wang, X. Cao, X. Wang, S. Yang, R. Wang, Electrochemical Oxidation and Determination of Glucose in Alkaline Media Based on Au (111)-Like Nanoparticle Array on Indium Tin Oxide Electrode, Electrochim. Acta. 138 (2014) 174-186.
[37] B.T. Draine, P.J. Flatau, Discrete-dipole approximation for scattering calculations, J. Opt. Soc. Am. A 11 (1994) 1491-1499.
[38] P. Zijlstra, P.M. Paulo, K. Yu, Q.H. Xu, M. Orrit, Chemical Interface Damping in Single Gold Nanorods and Its Near Elimination by Tip‐Specific Functionalization, Angew. Chem. Int. Ed. 124 (2012) 8477-8480.
[39] M. Chirea, S.S.E. Collins, X. Wei, P. Mulvaney, Spectroelectrochemistry of Silver Deposition on Single Gold Nanocrystals, J. Phys. Chem. Lett. 119 (2014) 4331-4335.

[40] A.M. Brown, M.T. Sheldon, H.A. Atwater, Electrochemical Tuning of the Dielectric Function of Au Nanoparticles, ACS Photonics 2, (2015) 459-464.
[41] S.K. Dondapati, M. Ludemann, R. Müller, S. Schwieger, A. Schwemer, B. Händel, D. Kwiatkowski, M. Djiango, E. Runge, T.A. Klar, Voltage-Induced Adsorbate Damping of Single Gold Nanorod Plasmons in Aqueous Solution, Nano Lett. 12 (2012) 1247-1252.
[42] O. Devereux, P. De Bruyn, The Effect of Specific Adsorption on the Interaction Energy between two Double Layers. 1. Theoretical Evaluation Based on the Grahame Model, J. Colloid. Sci. 19 (1964) 302-312.
[43] A. Henglein, Physicochemical Properties of Small Metal Particles in Solution: "Microelectrode" Reactions, Chemisorption, Composite Metal Particles, and the Atom-to-metal Transition, J. Phys. Chem. 97 (1993) 5457-5471.
[44] C. Jing, F.J. Rawson, H. Zhou, X. Shi, W.-H. Li, D.-W. Li, Y.-T. Long, New Insights into Electrocatalysis Based on Plasmon Resonance for the Real-Time Monitoring of Catalytic Events on Single Gold Nanorods, Anal. Chem. 86 (2014) 5513-5518.
[45] L. Burke, T. Ryan, The Role of Incipient Hydrous Oxides in the Oxidation of Glucose and Some of its Derivatives in Aqueous Media, Electrochim. Acta. 37 (1992) 1363-1370.
[46] R. Kötz, D. Kolb, J. Sass, Electron Density Effects in Surface Plasmon Excitation on Silver and Gold Electrodes, Surf. Sci. 69 (1977) 359-364.
[47] P.A. Kossyrev, A. Yin, S.G. Cloutier, D.A. Cardimona, D. Huang, P.M. Alsing, J.M. Xu, Electric Field Tuning of Plasmonic Response of Nanodot Array in Liquid Crystal Matrix, Nano Lett. 5 (2005) 1978-1981.
[48] V. Lioubimov, A. Kolomenskii, A. Mershin, D.V. Nanopoulos, H.A. Schuessler, Effect of Varying Electric Potential on Surface-plasmon Resonance Sensing, Appl. Opt. 43 (2004) 3426-3432.
[49] C. Langhammer, E.M. Larsson, B. Kasemo, I. Zorić, Indirect Nanoplasmonic Sensing: Ultrasensitive Experimental Platform for Nanomaterials Science and Optical Nanocalorimetry, Nano Lett. 10 (2010) 3529-3538.
[50] M. Hu, C. Novo, A. Funston, H. Wang, H. Staleva, S. Zou, P. Mulvaney, Y. Xia, G.V. Hartland, Dark-field Microscopy Studies of Single Metal Nanoparticles: Understanding the Factors that Influence the Linewidth of the Localized Surface Plasmon Resonance, J. Mater. Chem. 18 (2008) 1949-1960.
[51] C. Novo, D. Gomez, J. Perez-Juste, Z. Zhang, H. Petrova, M. Reismann, P. Mulvaney, G.V. Hartland, Contributions From Radiation Damping and Surface Scattering to the Linewidth of the

Longitudinal Plasmon Band of Gold Nanorods: a Single Particle Study, Phys. Chem. Chem. Phys. 8 (2006) 3540-3546.

[52] C. Langhammer, E.M. Larsson, B. Kasemo, I. Zoric, Indirect Nanoplasmonic Sensing: Ultrasensitive Experimental Platform for Nanomaterials Science and Optical Nanocalorimetry, Nano Lett. 10 (2010) 3529-3538.

[53] A. Pinchuk, U. Kreibig, A. Hilger, Optical Properties of Metallic Nanoparticles: Influence of Interface Effects and Interband Transitions, Surf. Sci. 557 (2004) 269-280.

[54] U. Kreibig, Interface-induced Dephasing of Mie Plasmon Polaritons, Appl. Phys. B: Lasers Opt. 93 (2008) 79-89.

[55] S. Paul, A. Chandra, Hydrogen Bond Dynamics at Vapour–water and Metal–water Interfaces, Chem. Phys. Lett. 386 (2004) 218-224.

[56] J.S. Gordon, D.C. Johnson, Application of an Electrochemical Quartz Crystal Microbalance to a Study of Water Adsorption at Gold Surfaces in Acidic Media, J. Electroanal. Chem. 365 (1994) 267-274.

[57] R. Chapman, P. Mulvaney, Electro-optical Shifts in Silver Nanoparticle Films, Chem. Phys. Lett. 349 (2001) 358-362.

[58] N. Liu, M.L. Tang, M. Hentschel, H. Giessen, A.P. Alivisatos, Nanoantenna-enhanced Gas Sensing in a Single Tailored Nanofocus, Nat. Mater. 10 (2011) 631-636.

[59] A. Liu, Q. Ren, T. Xu, M. Yuan, W. Tang, Morphology-controllable Gold Nanostructures on Phosphorus Doped Diamond-like Carbon Surfaces and their Electrocatalysis for Glucose Oxidation, Sens. Actuators, B: Chem. 162 (2012) 135-142.

[60] S.C. Warren, D.A. Walker, B.A. Grzybowski, Plasmoelectronics: Coupling Plasmonic Excitation with Electron Flow, Langmuir 28 (2012) 9093-9102.

[61] J.B. Sambur, P. Chen, Approaches to Single-Nanoparticle Catalysis, Annu. Rev. Phys. Chem. 65 (2014) 395-422.

[62] M. Eo, J. Baek, H.D. Song, S. Lee, J. Yi, Quantification of Electron Transfer Rates of Different Facets on Single Gold Nanoparticles During Catalytic Reactions, Chem. Commun. 49 (2013) 5204-5206.

[63] A. Hoggard, L.-Y. Wang, L. Ma, Y. Fang, G. You, J. Olson, Z. Liu, W.-S. Chang, P.M. Ajayan, S. Link, Using the Plasmon Linewidth To Calculate the Time and Efficiency of Electron Transfer between Gold Nanorods and Graphene, ACS Nano 7 (2013) 11209-11217.

[64] C. Sonnichsen, T. Franzl, T. Wilk, G. von Plessen, J. Feldmann, O. Wilson, P. Mulvaney, Drastic Reduction of Plasmon Damping in Gold Nanorods, Phys. Rev. Lett. 88 (2002) 077402.

[65] S. Link, M.A. El-Sayed, Size and Temperature Dependence of the Plasmon Absorption of Colloidal Gold Nanoparticles, J. Phys. Chem. B 103 (1999) 4212-4217.
[66] J. Olson, S. Dominguez-Medina, A. Hoggard, L.-Y. Wang, W.-S. Chang, S. Link, Optical Characterization of Single Plasmonic Nanoparticles, Chem. Soc. Rev. 44 (2015) 40-57.
[67] J. Fossey, W. Brittain, The CASE 2014 Symposium: Catalysis and Sensing for Our Environment, Xiamen 7 th–9 th November 2014. Org. Chem. Front. 2 (2015) 101-105.

Text and graphics for Table of Contents:

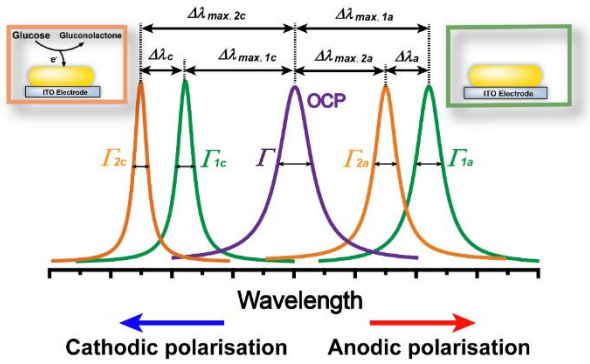

Graphical abstract

Highlights：

The electrocatalytic oxidation of glucose at single particle level is investigated for the first time.

Single-nanoparticle dark-field spectroelectrochemistry techniques are introduced.

High quality optical information is correlated with the electrochemical measurement for the heterogeneous electrocatalytic system.